Raman spectroscopy of orthorhombic $La_{1-x}Ca_xMnO_3$, x = 0.1-0.3

2001 J. Phys.: Condens. Matter 13 3741

(http://iopscience.iop.org/0953-8984/13/16/305)

INSTITUTE OF PHYSICS PUBLISHING JOURNAL OF PHYSICS: CONDENSED MATTER

J. Phys.: Condens. Matter **13** (2001) 3741–3752 www.iop.org/Journals/cm PII: S0953-8984(01)19611-6

Raman spectroscopy of orthorhombic $La_{1-x}Ca_xMnO_3$, $x = 0.1$–0.3

A E Pantoja[1,5], H J Trodahl[1], R G Buckley[2], Y Tomioka[3] and Y Tokura[3,4]

[1] School of Chemical and Physical Sciences, Victoria University of Wellington, PO Box 600, Wellington, New Zealand
[2] Industrial Research Limited, PO Box 31310, Lower Hutt, New Zealand
[3] Joint Research Centre for Atom Technology, Tsukuba 305-0046, Japan
[4] Department of Applied Physics, University of Tokyo, Tokyo 113-8656, Japan

E-mail: o.pantoja@irl.cri.nz (A E Pantoja)

Received 1 March 2001

Abstract

This paper reports polarization-resolved temperature-dependent Raman scattering measurements on single crystals of the orthorhombic perovskite colossal-magnetoresistive material $La_{1-x}Ca_xMnO_3$, with $x = 0.1, 0.275, 0.3$. It is demonstrated that two of the Raman lines undergo an anomalous softening as temperature is lowered through T_C, related to the development of magnetic order below ambient temperature. Also reported is the presence of second-order scattering, as has been previously predicted for the manganites. Only the broad features at 500 and 650 cm^{-1} that arise from disorder-induced scattering contribute to the second-order signal.

1. Introduction

Colossal-magnetoresistance (CMR) perovskite materials of the family $R_{1-x}A_xMnO_3$ (where R is a rare-earth metal: La, Pr, Nd, Dy; A is an alkaline earth: Sr, Ca, Ba, Pb) have gained prominence recently as they display a range of behaviours consistent with a strongly correlated electronic system. For instance, with changing temperature and/or hole doping by the A element they exhibit a range of magnetic behaviours, conductivity and insulating phases, charge ordering, and accompanying transitions between these states. Most interesting is the coincident conductivity and magnetic transition known as the CMR transition for the approximate range ($0.2 \leqslant x \leqslant 0.5$) in which the transition temperature T_C depends on the A-element doping [1].

Zener's double-exchange (DE) model [2] has provided a framework within which one can understand the CMR transition, although Millis *et al* [3] have recently pointed out that the DE model does not adequately explain the high resistance in the insulating phase above T_C. In this high-temperature region it has been argued that the carriers are coupled to the phonon system through a strong Jahn–Teller distortion known to exist in the end member $LaMnO_3$.

[5] Author to whom any correspondence should be addressed, at: Materials Physics, Industrial Research Limited, PO Box 31310, Lower Hutt, New Zealand.

0953-8984/01/163741+12$30.00

Recent data suggest further that the material is inhomogeneous, with coexisting regions of charge-ordered and charge-disordered phases at intermediate temperatures [4, 5].

These CMR manganites are perovskites, with distortions from perfect cubic symmetry. In the approximate cubic lattice there are no Raman-active phonons, so whether phonons appear at all in the spectra depends upon either the distortion or on the compositional disorder associated with the introduction of non-stoichiometric Ca. Raman scattering probes these lattice vibrations directly, and magnetic and charge-ordering effects indirectly.

In order to investigate the role of phonons in these transitions we have undertaken an extensive series of Raman spectroscopy measurements on single crystals of the CMR manganite $La_{1-x}Ca_xMnO_3$ (LCMO) for $x = 0.1$, 0.275, and 0.3 as a function of both polarization and temperature in the range 10–300 K. Recently, Liarokapis *et al* [6] investigated the Raman spectra of polycrystalline $La_{1-x}Ca_xMnO_3$ for $0 \leqslant x \leqslant 1$ from room temperature to 75 K. Irwin *et al* [7] have studied the temperature and oxygen-isotope-exchange dependence of the phonon lines seen for polycrystalline $La_{1-x}Ca_xMnO_3$ with $x = 0.2$, 0.35. Congeduti *et al* [8] have studied the pressure dependence of the Raman scattering in polycrystalline $La_{0.75}Ca_{0.25}MnO_3$ up to 14 GPa. Li *et al* [9] have studied the magnetostriction of polycrystalline $La_{0.75}Ca_{0.25}MnO_3$ up to 20 kOe.

Likewise, Granado *et al* [10] have studied the spectra of various members of the $R_{1-x}A_xMnO_3$ family, particularly the temperature dependence of polycrystalline $LaMnO_{3+\delta}$ [10, 11] and polycrystalline $(La_{1-y}Nd_y)_{2/3}Ca_{1/3}MnO_3$ ($y = 0$, 0.5, 1) [12]. Iliev *et al* [13] have carried out polarization-resolved studies of the parent compound $LaMnO_3$, complete with lattice dynamical calculations and symmetry mode assignments for the main observed modes. Single crystals of $R_{1-x}(Ca, A')_xMnO_3$ for R = (Pr, La), A′ = (Sr, Pb) have also recently been studied [14, 15]; these materials go through the same paramagnetic-to-ferromagnetic and insulating-to-metallic transition. These authors identified a definite difference between the electronic background behaviour above and below T_C. A range of Raman studies have also been reported on both single-crystalline and polycrystalline $La_{1-x}Sr_xMnO_3$ (LSMO) for $x \leqslant 0.3$ [16–19] and on thin-film $La_{0.7}Ca_{0.3}MnO_3$ with various substrates [20–22].

The material chosen for this study, $La_{1-x}Ca_xMnO_3$, is particularly attractive for the work because, unlike $La_{1-x}Sr_xMnO_3$, it displays the same distorted orthorhombic structure as is found in the parent compound. In the low-doped region, LSMO ($0.17 < x < 0.25$) and LCMO ($0.05 < x < 0.5$) display similar transport and spectroscopic results [1, 17–19, 23]. However, while LCMO is orthorhombic over that range, LSMO is rhombohedral (space group $R\bar{3}c$) and becomes orthorhombic only for $x \leqslant 0.17$ at $T = 300$ K and $x \leqslant 0.22$ at $T = 0$ K [23]. Our measured room temperature lattice parameters for these samples are similar to previously published single-crystal data [10, 24, 25] with the orthorhombic structure approaching pseudo-cubic or pseudo-tetragonal for $x \geqslant 0.25$. In general, the cell volume continues to contract at higher Ca doping, and with increasing Ca doping the lattice parameters a and c become almost equal for $0.1 \leqslant x \leqslant 0.5$. Although this may suggest that a better understanding of the structure in the low-doped region could come from a tetragonal symmetry analysis, as was previously noted [17] for $La_{0.7}Sr_{0.3}MnO_3$, we have treated these crystals using the orthorhombic $Pnma$ space group throughout this paper.

The orthorhombic perovskite phase of the parent $LaMnO_3$ has this same space group, and at the zone centre the following 60 phonon modes are allowed [13]:

$$\begin{aligned}\Gamma(Pnma) \equiv\ & 7A_g + 5B_{1g} + 7B_{2g} + 5B_{3g} && \text{(Raman active)}\\ & + 9B_{1u} + 7B_{2u} + 9B_{3u} && \text{(IR active)}\\ & + 8A_u && \text{(silent)}\\ & + B_{1u} + B_{2u} + B_{3u} && \text{(acoustic).}\end{aligned}$$

We have worked predominantly with the incident light parallel to the [010] direction, i.e. the y-axis, which gives access to the following symmetry configurations within the Porto notation (where the primed axes indicate a 45° rotation about the x–z plane):

$$z'z' \ (=x'x') \rightarrow A_g + B_{2g}$$
$$z'x' \ (=x'z') \rightarrow A_g$$
$$zz \ (=xx) \rightarrow A_g$$
$$zx \ (=xz) \rightarrow B_{2g}.$$

For the primed coordinates (x' and z') the incoming and detected light vectors are parallel to the Mn–O–Mn bonds in the cubic approximation to the structure.

2. Experimental details

The crystals used in the present study were prepared by the floating-zone method, the details of which are described elsewhere [26]. Part of a crystal was pulverized and characterized by means of powder x-ray diffraction, which confirmed that the crystal is single phase. The lattice parameters were obtained by Rietveld refinement of the powder XRD pattern. Resistivity was measured employing the conventional four-probe method. The magnetization data were derived from zero-field-cooled VSM measurements performed during warming in an external field of 0.1 T.

The cation ratios of the nominally $x = 0.1$ and $x = 0.275$ crystals were also checked by EPMA (electron probe microanalysis), which indicated that the Ca/(La + Ca) values analysed are actually 0.093 ± 0.002 and 0.265 ± 0.002 for those crystals respectively. The third crystal in our study ($x = 0.3$) has a Ca content of 0.29 ± 0.01, consistent with a decrease in x by about 0.01 from the pre-growth mixture. We quote the nominal values of x for the rest of this paper.

For the Raman experiments, samples were mounted in a variable-temperature closed-cycle refrigerator capable of reaching temperatures as low as 8 K. Raman measurements were performed on oriented crystals working from a polished (010) face. Polarized spectra were collected in the zz (xx), zx (xz), $z'z'$ ($x'x'$), and $z'x'$ ($x'z'$) configurations using the 514.5 nm line from an argon-ion laser and a Jobin-Yvon U1000 monochromator. The spectroscopic resolution selected was 4.5 cm^{-1}. Both point- and line-focus near-normal-incidence laser configurations were used. The point-focused illumination was kept at sufficiently low power ($\leqslant 12$ W mm^{-2}) to ensure that sample heating was kept to a minimum. The line-focus power density used was $\leqslant 0.3$ W mm^{-2}.

To test the local heating effect of the laser, the incident power was both increased and decreased from the values noted above while observing the sharpest line available (250 cm^{-1} in the $z'z'$ configuration), since its line position softens and its linewidth broadens as the local temperature is increased. Our results indicate that in the worst-case scenario (point-focus illumination) the temperature in the illuminated spot was no more than 40 K above that measured at the thermometer as 10 K. The thermal conductance of all of the elements in the cryostat increases with temperature, and at 200 K the temperature difference was estimated to be no more than 15–20 K. The power densities used here are much smaller than those for which Iliev *et al* [13] reported changes in the Raman spectra for stoichiometric $LaMnO_3$. Those changes were suggested to result from a transformation to the rhombohedral phase of $LaMnO_3$ at high laser powers. Irwin *et al* [7] have also reported an absence of power-density-related spectral effects, even at power densities as large as those used by Iliev *et al*. We speculate that the lower conductivity and relatively lower stability of the $x = 0$ orthorhombic phase is responsible for its sensitivity to high power levels.

3. Results and discussion

3.1. Polarization dependence

The major part of our results pertain to the crystal with $x = 0.275$ which shows a simultaneous resistive and magnetic transition at $T_C \sim 205$ K (figure 1). The change from insulating to metallic and from paramagnetic to ferromagnetic behaviour is very narrow, restricted to a region of no more than 15 K. This transition temperature is somewhat lower than has been reported [1] for LCMO near $x = 0.3$, possibly due to different firing processes. Note that Huang *et al* [24] reported a variation in the observed lattice parameters and T_C, following successive annealing of polycrystalline materials of the same Ca concentration. The $x = 0.3$ sample has a transition similar to that of the $x = 0.275$ sample with a T_C of 220 K and the $x = 0.1$ sample is insulating to low temperatures with a paramagnetic–ferromagnetic transition at 135 K.

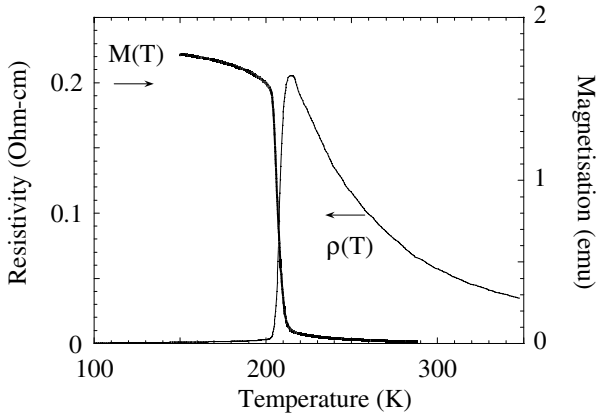

Figure 1. Temperature dependencies of the magnetization and resistivity for the single crystal of $La_{1-x}Ca_xMnO_3$ with $x = 0.275$.

In figure 2 we show the polarized Raman spectra of LCMO obtained at 295 K with $x = 0.275$ and $x = 0.1$. These curves, and all subsequent spectra, have been divided by the Bose–Einstein thermal factor $[n(\omega, T) + 1] = [1 - \exp(-\hbar\omega/k_BT)]^{-1}$ although the data that we display are not greatly affected by this correction below $T \sim 150$ K.

Like for published spectra for $La_{1-x}A_xMnO_3$ [6, 10, 14, 17, 19], the strongest features are two anomalously broad lines centred near 500 and 650 cm^{-1}, seen most clearly for the parallel polarization for $x = 0.1$ and for the $z'z'$ polarization for $x = 0.275$. The 650 cm^{-1} mode is actually a close doublet of two broad lines, as discussed further in the next section.

In addition to the very broad features, there are narrower A_g lines at 250 cm^{-1} in the parallel-polarized spectra ($z'z'$, zz) and at 450 cm^{-1} in the $z'x'$ and zz spectra. The 250 cm^{-1} line has been assigned to an out-of-phase rotational mode of oxygen atoms by Irwin *et al* [7] partly due to its strong oxygen-isotope effect. The 450 cm^{-1} mode remains unassigned, though Podobedov *et al* [19] identified it as of B_g symmetry due to its appearance in an xy spectrum. The almost flat amplitude of the zx spectrum of figure 2 shows that we observe no active B_{2g} modes within the *Pnma* space group, due to a comparatively small scattering cross section.

Finally, there is a very broad feature centred at 1100 cm^{-1} which we believe to be composed of weak second-order Raman scattering, mirroring the bands seen in the region 400–800 cm^{-1} at near twice the first-order frequency, as predicted by Allen and Perebeinos [27] for $LaMnO_3$.

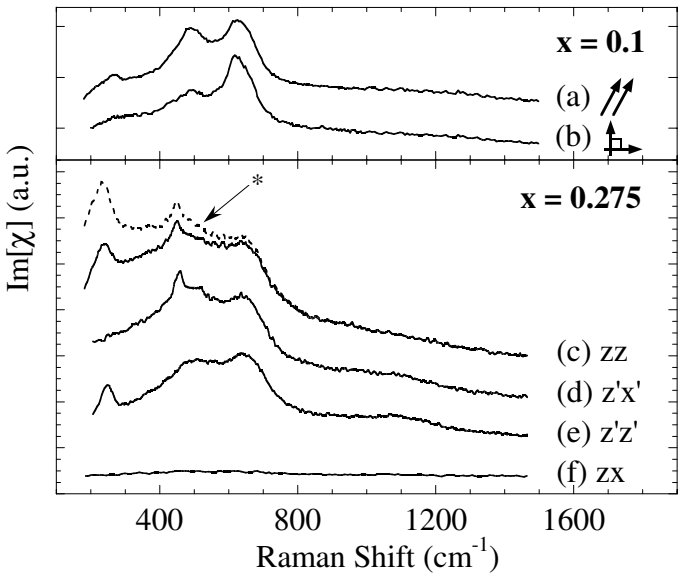

Figure 2. Polarized Raman spectra for $La_{1-x}Ca_xMnO_3$ at 295 K; $x = 0.1$ (top panel) and $x = 0.275$ (bottom panel). (a) Parallel polarized, (b) cross polarized, (c) zz (xx) A_g modes, (d) $z'x'$ $(x'z')$ weak A_g modes, (e) $z'z'$ $(x'x')$ $A_g + B_{2g}$ modes, and (f) zx (xz) B_{2g} modes. The dotted portion labelled $*$ gives an example of the data for zz (xx) polarization without the Bose–Einstein factor correction.

Such features in the range 800–1500 cm^{-1} have been seen in LSMO [16] for $x \leqslant 0.3$, in bi-layered $R_{2-2x}Sr_{1+2x}Mn_2O_7$ for R = Nd, Dy, Pr, La [28], in LCMO by Congeduti *et al* [8], and in a variety of materials by Yoon *et al* [14]. In that latter publication the higher-order scattering was assigned to scattering from small polarons. Their observed second-order scattering appears to be relatively strong in amplitude for materials with lower T_C. It is interesting to note in figure 2 that only the broad lines at ∼500 and ∼650 cm^{-1} are reflected at higher frequency; the sharper bands at 250 cm^{-1} and 450 cm^{-1} are not. Further details on this second-order scattering have been published elsewhere [28].

3.2. Temperature dependence

Figure 3 shows a selection of curves for the $x'z'$ and $z'z'$ polarizations for the $x = 0.275$ sample as functions of temperature. In order to estimate the line parameters and temperature dependencies of the observed lines shown in figure 3, they were fitted with a sum of Lorentzians: 250 cm^{-1} for $z'z'$ or 445 cm^{-1} for $z'x'$, 500 cm^{-1}, 640 cm^{-1}, 670 cm^{-1}, and one at 1100 cm^{-1} representing the sum of the second-order scattering. In addition we fit a slowly varying electronic background rising toward zero frequency [14, 15]. Unlike the earlier studies, we see no evidence in our spectra of a change in this electronic background when the sample goes from the paramagnetic/insulating to ferromagnetic/metallic phases. Note, however, that we have no data below ∼180 cm^{-1} where this change will be most noticeable.

From a simple inspection of figure 3 it can be noted that the two broad 500 cm^{-1} and 650 cm^{-1} modes in the $z'x'$ spectra (top panel) have the strongest temperature dependence, narrowing and growing in strength with falling temperature. The narrowing of the 500 cm^{-1} Mn–O bending mode is as expected for an anharmonic-scattering limited phonon lifetime, but

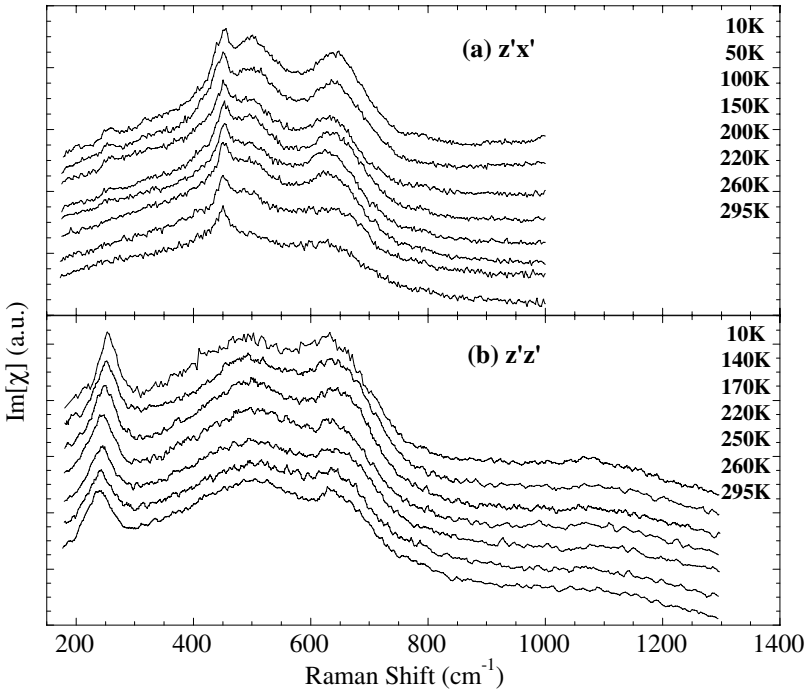

Figure 3. Temperature dependences of the $x = 0.275$ LCMO sample; (a) $z'x'$ polarization and (b) $z'z'$ polarization. The spectra have been offset and normalized for clarity.

the strengthening is unusual. For the parallel $z'z'$ polarization (bottom panel) this mode is nearly twice as wide as it is for $z'x'$ polarization; it is far less distinct, and it can be seen to not change at all with temperature.

As mentioned previously, the line at 650 cm^{-1} appears to be a doublet made up of lines near 630 and 670 cm^{-1} as shown in figure 4. The plot clearly shows this relationship for the sample with $x = 0.1$. This speculation is supported by the fact that for the stoichiometric parent $LaMnO_3$ [13, 19] two lines are indeed seen in that region, at 610 cm^{-1} and 670 cm^{-1}. The intensity of the ∼650 cm^{-1} doublet weakens rapidly as x is increased to ∼0.3 [6] since the structure becomes progressively more cubic in that doping region [10, 24, 25]. The fact that there are two lines in the 650 cm^{-1} region can also account for the weak asymmetry which can be seen in this shoulder feature. The inset in figure 4 displays the temperature dependence of the two lines in the doublet for the $x = 0.275$ crystal, showing that the lines clearly remain split by about 40 cm^{-1} down to low temperatures. Both lines also show an anomalous softening similar to that seen in the 450 cm^{-1} line of LCMO (figure 5) at T_C and in the 610 cm^{-1} line of the stoichiometric parent compound at T_N [11]. We speculate that the softening is thus associated with the magnetic ordering at T_C. Significantly, we do not see a minimum in the width of this compound feature (or a maximum in its intensity) coinciding with T_C as was seen by Abrashev *et al* [20] for thin-film LCMO. The changes in width and amplitude are monotonic with temperature.

This compound feature near 650 cm^{-1} seems to narrow for $z'x'$ polarization at lower temperature, but broaden for $z'z'$ polarization (figure 3). The fact that there are two independent lines in this region explains this apparent contradiction: the two lines slightly diverge at low temperatures (inset, figure 4), causing the apparent widening for $z'z'$ polarization. For $z'x'$

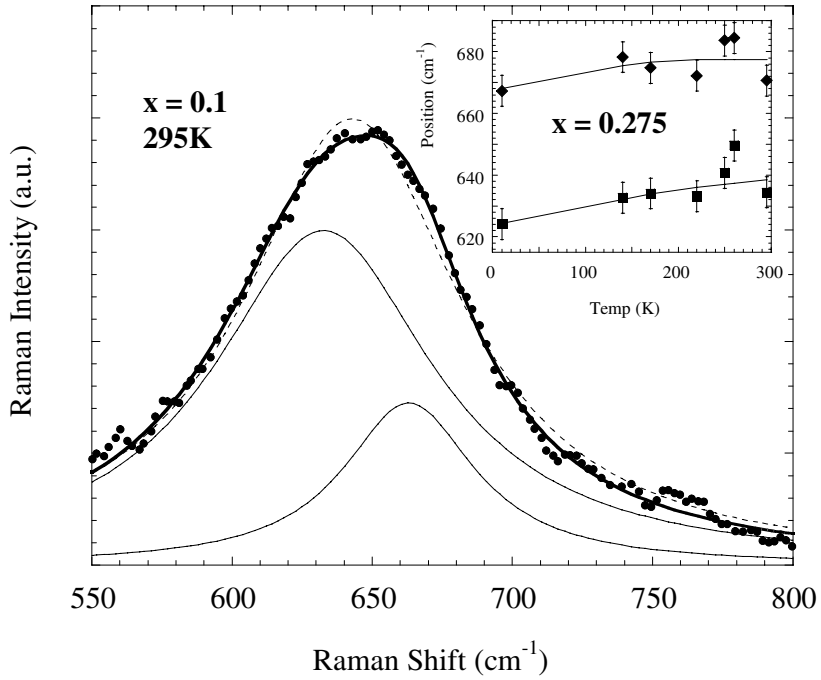

Figure 4. A doublet representation of the broad 650 cm^{-1} feature. *Main plot:* the $x = 0.1$ sample for crossed polarization at ambient temperature. Solid circles: Raman data with the other curve fit components subtracted. Solid lines: two Lorentzian phonon lines making up the doublet, and their sum. Dashed line: a single-phonon Lorentzian fit to the data. *Inset:* the line positions of the close doublet (diamonds and squares) versus temperature for the $x = 0.275$ sample for $z'z'$ polarization.

polarization one line appears stronger than the other by virtue of the different polarization selection rules.

Looking now at the narrower 250 and 450 cm^{-1} lines in figure 3, the temperature dependencies have been derived from single-Lorentzian fits, with the line positions shown in figure 5. For the 250 cm^{-1} $z'z'$ line (top panel, solid circles) there is a hardening of about 9 cm^{-1}, approximately 3.5%, between ambient temperature and 10 K. The effect is exactly as expected from thermal contraction. In the top panel of figure 5 we show a curve fit to the line position of a simple anharmonic potential model for the thermal contraction effect [29]:

$$\omega(T)_{\text{anh}} = \omega(0)(1 + 2[n(\omega, T) + 1]) + \text{constant}. \tag{1}$$

Here $\omega(0)$ is the line position at $T = 0$. As seen, the agreement between the data and equation (1) is excellent. We have also carried out a fit to the 250 cm^{-1} line's position with a model given by Lee and Min [30,31] which relates the temperature dependence of the phonon frequency to a correlation-affected ionic restoring force in the DE model using the mean-field approximation of Kubo and Ohata [32]. This model provided a clearly inferior fit to the data. In particular there is no evidence in the data of a discontinuous change in the temperature derivative of the frequency at the Curie temperature as predicted by the DE model at zero field. Our 9 cm^{-1} shift is nearly identical to that reported for $x = 0.35$ by Irwin *et al* [7] but the discontinuity at T_C is missing. We note in this regard that the present material has a Curie temperature a full 80 K below ambient temperature, so we have accessed a greater range above T_C than was the case in the earlier work.

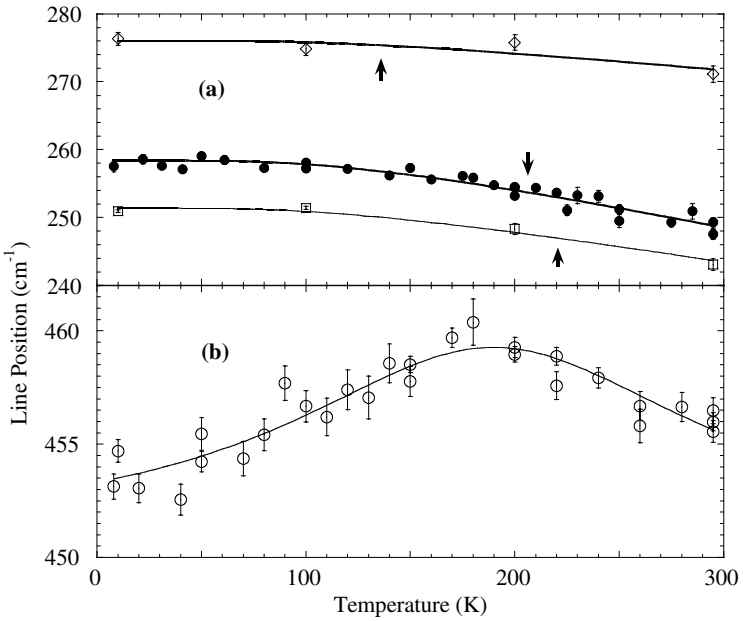

Figure 5. The dependence of the line position for the two sharpest features observed as a function of temperature. (a) $x = 0.1$, unpolarized (diamonds); the 250 cm^{-1} line for $x = 0.275$ for $z'z'$ polarization (solid circles) and for $x = 0.3$ unpolarized (squares); and (b) the 450 cm^{-1} line for $x = 0.275$ for $z'x'$ polarization. The top-panel data have simple anharmonic curves fitted (see the text), and in the bottom panel the line is a guide to the eye. The arrows indicate the magnetic transition.

For comparison we also show in figure 5 the measured oxygen line frequencies for two other samples with Ca concentrations of $x = 0.1$ and $x = 0.3$. We see that the frequency of this feature is lowered by the Ca content, as reported by others [7, 17, 19]. This dramatic change in phonon frequency ($\sim$30 cm^{-1} for $0 \leqslant x \leqslant 0.3$) caused by ionic A-site substitution has been associated with the change in the atomic radius $\langle r_A \rangle$ [7].

We turn next to the line at 450 cm^{-1}, seen for crossed polarization (figure 5(b)). The temperature dependence of this mode is anomalous, for the normal hardening reverses as the temperature falls below T_C; there is a pronounced softening which apparently sets in just below the Curie temperature. A plausible $\sim$15 K of local sample heating could be responsible for the apparent mismatch between the magnetic transition (figure 1) and the temperature at which the frequency of this line peaks. Spectra taken for our $x = 0.3$ LCMO crystal also display the same anomalous temperature-dependent behaviour as is seen in figure 5(b), but with the line at 447 cm^{-1}.

Note that a similar anomalous softening appears in the Mn–O bending and stretching modes at 490 cm^{-1} (A_g) and 610 cm^{-1} (B_{2g}) of $LaMnO_3$ at T_N [10, 11, 19] although there is no metal–insulator transition in this material. Interestingly, something similar is seen in the nominally 324 cm^{-1} B_{1g} phonon of bi-layered manganite $La_{1.2}Sr_{1.8}Mn_2O_7$ which is known to have a metal–insulator transition near 120 K [33]. Thus this softening phenomenon is clearly related to the magnetic transition in these and similar materials, and independently appears irrespective of the existence of the metal–insulator transition. It is tempting to associate the softening with a spin correlation effect in the inter-ionic interaction, similar but of opposite sign to that suggested for the 230 cm^{-1} line by Irwin *et al* [7]. Within

this model the frequency decrement is expected to follow the nearest-neighbour spin–spin correlation function. However, our observed temperature dependence is in disagreement with the prediction of a cusp-like fall at T_C, levelling off at lower temperature, which results from this picture. We suggest instead that the continued softening below T_C is indicative of a continued structural change in the crystal in that temperature range. The obvious candidates are the reported changing balance between regions of ordered and non-ordered Mn–O bond-length variations [4] and the coexistence of a mixed ferromagnetic–metallic and insulating phase at low temperatures [5].

3.3. Mode assignments

In the absence of any lattice dynamical calculations for any but the stoichiometric form of this material, the mode assignments in this and most earlier publications must be based primarily on a comparison with that parent compound [13, 14, 17, 19]. Thus as a guide to the mode assignments, and for a more complete comparison with earlier single-crystal results, we plot in figure 6 the main observed line frequencies as a function of Ca concentration x. Where available, the symmetries of the modes are noted, as determined from the polarization dependencies of the scattering.

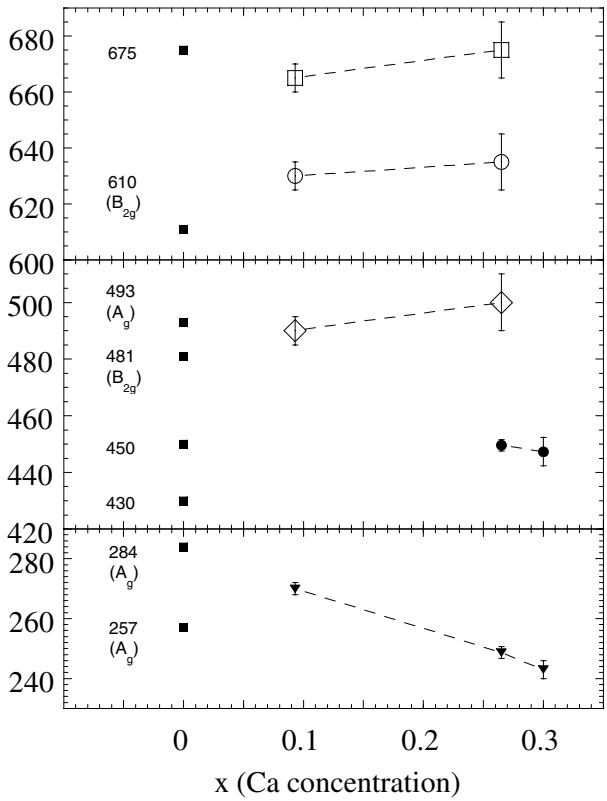

Figure 6. Observed line positions of all of the A_g features in LCMO for $\omega \leqslant 1000$ cm^{-1} as a function of the Ca concentration at room temperature. The solid squares along the line $x = 0$ are the observed modes in $LaMnO_3$ from references [13] and [19] with corresponding frequencies and symmetries.

We have used only single-crystal data for the assignments, as effects from annealing and substrate lattice strain in thin-film samples [20–22] and that of grain boundaries on polycrystalline samples [6, 7, 19] would add to the ambiguity of the assignments.

Extrapolation of the 250 cm^{-1} mode to zero concentration would suggest that it is identical to the 284 cm^{-1} line seen [13] for $LaMnO_3$ and assigned as an A_g out-of-phase rotation of the oxygen cage. This extrapolation thus confirms the assignment of Irwin *et al* [7] for the 250 cm^{-1} mode in LCMO.

The line of A_g symmetry at 450 cm^{-1} cannot correspond to the 481 cm^{-1} line seen for stoichiometric $LaMnO_3$, as that is a B_{2g} mode. Liarokapis *et al* [6] do see a sharp line near 430 cm^{-1} for $x = 0.3$, but we do not believe that it is the same sharp line as we see in figure 5(b), as the line that they see grows in strength markedly with lower temperature and it is too low in frequency. We suggest that the line that we see is the same as that seen at 450 cm^{-1} for $LaMnO_3$ by Podobedov *et al* [19] although no mode symmetry was given in that earlier report. Iliev *et al* [13] do not observe a mode at this frequency in $LaMnO_3$ and without further studies on similar single crystals this mode must remain unassigned for now.

The three strong and unusually broad modes at 500, 630, and 670 cm^{-1} are difficult to assign to any specific zone-centre vibrations. We have previously argued [28] that the modes seen in the 400–800 cm^{-1} region of the *layered* manganites are a mixture of sharp zone-centre modes (as is usual for polarization-dependent lines) and broad non-zone-centre modes from a full optical branch, rendered active through the disorder introduced by the non-stoichiometry of A-site doping. This is also likely to be the case for the three broad modes that we observe in LCMO in the region 400–800 cm^{-1}. For example, the first mode of the doublet in figure 4 at nominally 630 cm^{-1} could be assigned to the B_{2g} in-phase stretching mode seen in the parent compound [13] at 611 cm^{-1}, were it not for the fact that no modes appear in the B_{2g} xz spectrum of figure 2. This apparent contradiction disappears if we consider this mode to be a result of disorder-induced scattering from a full branch, for which the usual polarization selection rules do not apply. Finally, the broad mode at 500 cm^{-1} has been previously assigned [13] to an A_g bending mode of the Mn–O_6 octahedra, but its width could also result from full-branch scattering.

4. Conclusions

We have presented a complete set of temperature-dependent Raman spectra for single crystals of $La_{1-x}Ca_xMnO_3$, for nominal x-values of 0.1, 0.275, and 0.3. In agreement with most earlier studies, we see two broad features between 400 and 800 cm^{-1} in most polarization configurations, and two lines with more complex polarization dependence and of more conventional width near 250 and 450 cm^{-1}. We can resolve the higher-frequency broad line into two, centred near 630 and 670 cm^{-1}.

The line at 250 cm^{-1} shows a temperature dependence which is entirely conventional within the usual anharmonic picture, with no change in its behaviour near the magnetic/metallic transition. Both the 450 cm^{-1} line and the doublet near 650 cm^{-1} anomalously soften in the two crystals with x near 0.3 as the temperature is reduced below ambient, and the softening in the 450 cm^{-1} line is clearly seen to have an onset near the transition temperature. The anomalous behaviour is probably due to changing electronic states as inhomogeneous magnetic order increases below the transition.

Second-order scattering is observed in LCMO for the first time, as has been predicted to occur in the presence of the Jahn–Teller effect in these materials. It is noted that only the broad lines that arise from disorder-induced scattering are present in the second-order scattering.

Acknowledgments

We would like to thank S Rupp for the magnetization measurements, and AEP is indebted to O Mercier and M Howard for valuable discussions. This research was in part supported by the New Zealand Marsden Fund and by NEDO in Japan.

References

[1] Ramirez A P 1997 *J. Phys.: Condens. Matter* **9** 8171
Imada M, Fujimori A and Tokura Y 1998 *Rev. Mod. Phys.* **70** 1039
[2] Zener C 1951 *Phys. Rev.* **82** 403
[3] Millis A J, Littlewood P B and Shraiman B I 1995 *Phys. Rev. Lett.* **74** 5144
[4] Lanzara A, Saini N L, Brunelli M, Natali F, Bianconi A, Radaelli P G and Cheong S-W 1998 *Phys. Rev. Lett.* **81** 878
[5] Jaime M, Lin P, Chun S H, Salamon M B, Dorsey P and Rubinstein M 1999 *Phys. Rev.* B **60** 1028
Papavassiliou G, Fardis M, Belesi M, Maris T G, Kallias G, Pissas M, Niarchos D, Dimitropoulos C and Dolinsek J 2000 *Phys. Rev. Lett.* **84** 761
[6] Liarokapis E, Leventouri Th, Lampakis D, Palles D, Neumeier J J and Goodwin D H 1999 *Phys. Rev.* B **60** 12 758
[7] Irwin J C, Chrzanowski J and Franck J P 1999 *Phys. Rev.* B **59** 9362
[8] Congeduti A, Postorino P, Caramagno E, Nardone M, Kumar A and Sarma D D 2001 *Phys. Rev. Lett.* **86** 1251
[9] Li J H, Huan C H A, Du Y-W, Feng D and Shen Z X 2000 *Phys. Rev.* B **63** 024416
[10] Granado E, Moreno N O, García A, Sanjurjo J A, Rettori C, Torriani I, Oseroff S B, Neumeier J J, McClellan K J, Cheong S-W and Tokura Y 1998 *Phys. Rev.* B **58** 11 435
[11] Granado E, García A, Sanjurjo J A, Rettori C, Torriani I, Prado F, Sánchez R D, Caneiro A and Oseroff S B 1999 *Phys. Rev.* B **60** 11 879
[12] Granado E, García A, Sanjurjo J A, Rettori C and Torriani I 2001 *Phys. Rev.* B **63** 064404
[13] Iliev M N, Abrashev M V, Lee H-G, Popov V N, Sun Y V, Thomsen C, Mens R L and Chu C W 1998 *Phys. Rev.* B **57** 2872
[14] Yoon S, Liu H L, Schollerer G, Cooper S L, Han P D, Payne D A, Cheong S-W and Fisk Z 1998 *Phys. Rev.* B **58** 2795
[15] Liu H L, Yoon S, Cooper S L, Cheong S-W, Han P D and Payne D A 1998 *Phys. Rev.* B **58** 10 115
[16] Björnsson P, Rübhausen M, Bäckström J, Käll M, Eriksson S, Eriksen J and Börjesson L 2000 *Phys. Rev.* B **61** 1193
[17] Podobedov V B, Weber A, Romero D B, Rice J P and Drew H D 1998 *Solid State Commun.* **105** 589
[18] Gupta R, Sood A K, Mahesh R and Rao C N R 1996 *Phys. Rev.* B **54** 14 899
[19] Podobedov V B, Weber A, Romero D B, Rice J P and Drew H D 1998 *Phys. Rev.* B **58** 43
[20] Abrashev M V, Ivanov V G, Iliev M N, Chakalov R A, Chakalova R I and Thomsen C 1999 *Phys. Status Solidi* b **215** 631
[21] Malde N, Desilva P S I P N, Hossain A K M A, Cohen L F, Thomas K A, MacManus-Driscoll J L, Mathur N D and Blamire M G 1998 *Solid State Commun.* **105** 643
[22] Podobedov V B, Romero D B, Weber A, Rice J P, Schreekala R, Rajeswari M, Ramesh R, Venkatesan T and Drew H D 1998 *Appl. Phys. Lett.* **73** 3217
[23] Okuda T, Tomioka Y, Asamitsu A and Tokura Y 2000 *Phys. Rev.* B **61** 8009
Ivanshin V A, Deisenhofer J, Krug von Nidda H-A, Loidl A, Mukhin A A, Balbashov A M and Eremin M V 2000 *Phys. Rev.* B **61** 6213
Dabrowski B, Xiong X, Bukowski Z, Dybzinski R, Klamut P W, Siewenie J E, Chmaissem O, Shaffer J, Kimball C W, Jorgensen J D and Short S 1999 *Phys. Rev.* B **60** 7006
Mitchell J F, Argyriou D N, Potter C D, Hinks D G, Jorgensen J D and Bader S D 1996 *Phys. Rev.* B **54** 6172
[24] Huang Q, Santoro A, Lynn J W, Erwin R W, Borchers J A, Peng J L, Ghosh K and Greene R L 1998 *Phys. Rev.* B **58** 2684
[25] Subías G, García J, Blasco J and Proietti M G 1998 *Phys. Rev.* B **58** 9287
[26] Tomioka Y, Asamitsu A and Tokura Y, unpublished
[27] Allen P B and Perebeinos V 1999 *Phys. Rev. Lett.* **83** 4828
Perebeinos V and Allen P B 2000 *Preprint* cond-mat/0007301
[28] Pantoja A E, Trodahl H J, Fainstein A, Pregliasco R G, Buckley R G, Balakrishnan G, Lees M R and Paul D M^{c}K 2001 *Phys. Rev.* B **63** 132 406

[29] See, for instance, Roy C and Budhani R C 1998 *Phys. Rev.* B **58** 8174
[30] Lee J D and Min B I 1997 *Phys. Rev.* B **55** 12 454
[31] Yu U, Min B I and Lee J D 2000 *Phys. Rev.* B **61** 84
[32] Kubo K and Ohata N 1972 *J. Phys. Soc. Japan* **33** 21
[33] Romero D B, Podobedov V B, Weber A, Rice J P, Mitchell J F, Sharma R P and Drew H D 1998 *Phys. Rev.* B **58** 14 737